




Generation of a quasi-chirp-free short isolated attosecond pulse from high-order harmonics by optimized multicolor laser fields

Jin-Xu Du,¹ Guo-Li Wang ,^{1,*} Xiao-Yong Li,² Zhi-Hong Jiao ,¹ Song-Feng Zhao,^{1,†} and Xiao-Xin Zhou ^{1,3,‡}

¹College of Physics and Electronic Engineering, Northwest Normal University, Lanzhou 730070, China

²Department of Experimental Teaching, Northwest Minzu University, Lanzhou, 730030, China

³Beijing National Laboratory for Condensed Matter Physics, Institute of Physics, Chinese Academy of Sciences, Beijing 100190, China



(Received 10 April 2023; accepted 12 July 2023; published 1 August 2023)

A chirped isolated attosecond pulse (IAP) will be usually produced if several chirped supercontinuum high-order harmonics are coherently superposed. Thus, to generate a broad bandwidth quasi-chirp-free IAP or even short isolated subattosecond pulse, one needs to reduce the attosecond chirp (attochirp) of high-order harmonic pulses. In this paper, we theoretically demonstrate the possibility of generating the quasi-chirp-free IAP from neon atom driven by the optimized four-color laser field, which is synthesized by two fundamental near-infrared lasers and their second-harmonic fields. By increasing the colors in synthesized field from two or three to four, the attochirp of broadband high-order harmonics over 100 eV is significantly reduced, and the generated IAP is shortened from more than 50 attosecond (as) to 37 as, approaching the Fourier-transform-limited pulse duration of 36 as. The classical analysis reveals that this mainly stems from the simultaneous return of electrons ionized at different times to the parent ion, as has been shown from other investigations regarding the necessity of producing attochirp-free high harmonics with multicolor laser fields. Most importantly, such short quasi-chirp-free isolated IAP survives after the macroscopic propagation effects are carried out, under proper gas pressure and laser beam waist. This work provides an efficient method for experiments to generate the quasi-chirp-free IAPs by using the synthesized and optimized four-color laser field.

DOI: [10.1103/PhysRevA.108.023101](https://doi.org/10.1103/PhysRevA.108.023101)

I. INTRODUCTION

Isolated attosecond pulse (IAP) provides a robust tool for studying ultrafast processes of electrons inside atoms and molecules [1–6], such as real-time probing ultrafast dynamics of electrons in inner-shell levels of atoms, tunneling ionization of electrons in a laser field, and the attosecond transient absorption and Fano resonance. Since high-order harmonics from atoms and molecules in intense laser fields has a very wide spectral width covering from extreme ultraviolet (XUV) to soft x rays [7], it has become the most popular way to obtain attosecond pulses experimentally [8,9]. The process of high-order harmonic generation (HHG) can be well understood in terms of the three-step model [10,11], namely the electron first tunnels through the barrier formed by the Coulomb potential and the laser field, then it oscillates quasi-freely driven by the laser field and acquires additional kinetic energy, finally it can recombine with the parent ion and emit a high-energy photon.

So far, a variety of gating techniques have been proposed and employed for the IAP generation, such as the amplitude gating [12], ionization gating [13], polarization gating [14], double-optical gating [15,16], and attosecond lighthouse [17,18]. For example, Goulielmarkis *et al.* [12] reported an 80 as IAP obtained by the amplitude gating technique using

carrier-envelope phase (CEP) stabilized few-cycle laser field. Then, Li *et al.* [14] produced a 53 as IAP with the polarization gating technique. In the same year, Gaumnitz *et al.* [19] reported a 43 as pulse with a bandwidth of about 100 eV and photon energy up to 180 eV with CEP stabilized midinfrared (MIR) laser.

In recent years, MIR lasers have been widely used to obtain high-order harmonics in the keV x-ray region. For example, Popmintchev *et al.* [7] generated the bright harmonic spectra with 1.6 keV band width from high-pressure noble gases by a MIR femtosecond laser, which facilitates the generation of the Fourier-transform-limited pulse close to 2 as. However, theoretical and experimental studies have confirmed that the relation between the conversion efficiency of HHG and the driving pulse wavelength is $\lambda^{-(5-6)}$ [20,21]. Therefore, the cost of employing a MIR laser for extending the continuous harmonic spectrum is the loss of emission efficiency. Fortunately, an advanced technique of laser field coherent synthesis has been developed to obtain a laser pulse with the arbitrary waveform [22–29]. It is found that multicolor linearly polarized laser fields with the same polarization direction can significantly enhance the harmonic yield and extend the cutoff energy [30,31]. More importantly, the optimized multicolor lasers have also been used to produce IAPs [32–34]. As an important progress, in our recent work [35], we have demonstrated that the CEP for optimized multicolor fields does not influence the width and intensity of IAPs.

According to the semiclassical three-step model [10,11], the ionized electrons with different kinetic energies may come

*Corresponding author: wanggl@nwnu.edu.cn

†Corresponding author: zhaosf@nwnu.edu.cn

‡Corresponding author: zhouxx@nwnu.edu.cn

back to the parent core at different times, which leads to the so-called attochirp [36]. Therefore, the duration of attosecond pulses generated by gating techniques is usually longer than that of the Fourier-transform-limited pulse. To shorten the attosecond pulse, one can employ external phase corrections to compensate the harmonic chirp, including employing the negative group delay dispersion materials [36–38], using chirped multilayer x-ray mirrors [39]. On the other hand, from the single-atom level, one can engineer harmonic phases during their generation process with multicolor laser fields [40–42], which is inspired by the well-known knowledge that the temporal prole of attosecond burst is the shortest when the phase difference between two consecutive harmonics is constant. Theoretically, Kohler *et al.* [41] showed that the full compensation of attosecond chirp can be achieved by shaping the laser pulse with at least eight-color laser fields. However, it is very challenging to synthesize an eight-color laser in experiments. Very recently, Yu *et al.* [42] generated 251-as quasi-chirp-free isolated attosecond pulses with orthogonal two-color fields. One important conclusion from Refs. [41,42] is that electrons in the laser field, which start into the continuum at different times should revisit the ionic core at the same time. Producing shorter chirp-free isolated attosecond pulses is still urgently needed. In this paper, we propose an efficient method for generating the quasi-chirp-free high-order harmonics and IAPs by using a four-color laser pulse. We emphasize that the present optimized four-color laser is much easier to realize in experiments by synthesizing two fundamental infrared lasers and their second harmonic fields. A quasi-chirp-free IAP with pulse duration down to 37 as is obtained both in the single-atom response and macroscopic level. The present method would shed more lights on the generation of chirp-free ultrashort IAPs or even isolated subattosecond pulses in experiments.

The paper is organized as follows. In Sec. II, we will give a brief introduction to our theoretical methods on how to synthesize and optimize the multicolor laser field, and how to calculate the single and macroscopic HHG, namely, the strong-field approximation model, and solving the three-dimensional propagation equations, respectively. In Sec. III, we will investigate the influence of the number of components in a synthesized driving field on the emission of single-atom high-order harmonics and corresponding attosecond pulses, and conclude that the quasi-chirp-free short IAP can be obtained by using an optimized four-color laser pulse. We then study the effect of propagation on the attochirp of high-order harmonic pulses. The conclusion will be given in Sec. IV.

II. THEORETICAL METHODS

A. Optimization of laser waveform

The form of the driven laser field with multicolor coherent synthesis can be written as

$$E(t) = \sum_{i=1}^n E_i f(t - t_{di}) \cos[\omega_i(t - t_{di}) + \varphi_i], \quad (1)$$

where E_i is the electric field amplitude, $f(t) = e^{-2 \ln 2 t^2 / \tau^2}$ is the Gaussian pulse envelope, τ is the pulse duration [full width at half-maximum (FWHM)], ω_i is laser angular frequency, φ_i

is CEP, and t_{di} is relative time delay. In the optimization process, we take $t_{d1} = 0$ and $\varphi_i = 0$. If a two-color field ($n = 2$) is employed, wavelengths of the laser are taken to be $\lambda_1 = 800$ nm and $\lambda_2 = 1300$ nm, respectively. We mention that these two fundamental near-infrared lasers are available in many ultrafast laboratories. In the case of a three- or four-color fields ($n = 3$ or 4), we propose to add two second-harmonic fields (i.e., $\lambda_3 = 650$ nm, $\lambda_4 = 400$ nm) of those two fundamental lasers, given that second harmonics can be easily obtained by using nonlinear optical crystals in experiments. In this paper, we fix the FWHM of each color in the synthesized four-color laser field as 16 fs. The other parameters (E_i , τ_i) are obtained by optimizing the fitness function with the genetic algorithm (GA). The search space of τ_i is limited in $[-3$ fs, 3 fs]. Since the GA is a very efficient optimization algorithm for searching unknown multiple parameters, it has been widely used in the study of strong field phenomena [43–45]. It starts with a population of randomly generated individuals, then better individuals selected from the current generation by evaluating value of the fitness function of each individual are used in the next generation. In our optimization, we choose the number of iteration and population size as 3000 and 10, respectively. The fitness function in the optimizations is defined as

$$F = \frac{I_1}{I_2 \times \Delta\tau}, \quad (2)$$

where I_1 is the pulse intensity of the desired IAP generated from the single-atom response, I_2 is the other attosecond pulse intensity, and $\Delta\tau$ is the width of the target attosecond pulse.

B. Strong-field approximation theory

We theoretically investigate high-order harmonic emission from neon atoms driven by a multicolor laser field based on the strong field approximation (SFA) theory [46,47]. The time-dependent induced dipole moment has the following form:

$$\begin{aligned} D(t) = & i \int_{-\infty}^{\infty} d\tau \left(\frac{\pi}{\varepsilon + i\tau/2} \right)^{3/2} d^*[p_{st}(t, \tau) + A(t)] \\ & \times a^*(t) e^{-iS_{st}(t, \tau)} d[p_{st}(t, \tau) + A(t - \tau)] \\ & \times E(t - \tau) a(t - \tau) + \text{c.c.}, \end{aligned} \quad (3)$$

where $A(t)$ is the vector potential of laser pulse, $a(t) = \exp[-\frac{1}{2} \int_{-\infty}^t \omega(\tau) d\tau]$ is the ground-state amplitude of atoms, the ionization rate $\omega(\tau)$ can be calculated by the Ammosov-Delone-Krainov (ADK) model [48,49], and $d(p) = i^{2l/2} (2I_p)^{5/4} \frac{p}{(p^2 + 2I_p)^3}$ is the field-free dipole transition matrix element for transitions from the ground state to the continuum state characterized by a momentum p , I_p is the ionization potential. p_{st} and S_{st} are the stationary momentum and quasiclassical action given by

$$p_{st}(t, \tau) = -\frac{1}{\tau} \int_{t-\tau}^t dt'' A(t''), \quad (4)$$

$$S_{st}(t, \tau) = \int_{t-\tau}^t dt'' \left\{ \frac{1}{2} [p_{st} + A(t'')]^2 + I_p \right\}, \quad (5)$$

where $I_p = 21.6$ eV is the ionization potential of neon atom. The high-order harmonic spectra can be obtained by $S(\omega) \propto \omega^4 |D(\omega)|^2$ with $D(\omega)$ is the Fourier transform of the time-dependent induced dipole moment $D(t)$. By superimposing harmonics in a certain energy range, the single-atom attosecond pulse is obtained,

$$I(t) = \left| \sum_q a_q e^{iq\omega t} \right|^2, \quad (6)$$

where $a_q = \int D(t) e^{-iq\omega t} dt$.

C. Propagation equations

In view of the macroscopic level, high-order harmonics are emitted from a large number of neon atoms. At the same time, the nature of the laser beam is affected by the plasma formed from the ionized gas. Therefore, the propagation of laser pulses and high-order harmonics in a gas medium have to be considered after the quasi-chirp-free high-order harmonics and IAP are obtained from the single-atom response. If the laser electric field distribution in the interaction region is $E_l(r, z, t)$, its evolution in the atomic gas medium is given by the three-dimensional (3D) Maxwell's wave equation [50–54]

$$\begin{aligned} \nabla^2 E_l(r, z, t) - \frac{1}{c^2} \frac{\partial^2 E_l(r, z, t)}{\partial t^2} \\ = \mu_0 \frac{\partial J_{\text{abs}}(r, z, t)}{\partial t} + \frac{\omega_0^2}{c^2} (1 - \eta_{\text{eff}}^2) E_l(r, z, t), \end{aligned} \quad (7)$$

where z is the direction of laser propagation, and $J_{\text{abs}}(t) = \frac{\omega(t)n_e(t)I_p E_l(t)}{|E_l(t)|^2}$ is the absorption term due to the ionization of the medium [50,55], with the ionization rate $\omega(t)$ and free electron density $n_e(t)$ calculated by the ADK theory [48,49]. The effective refractive index of the gas medium is

$$\eta_{\text{eff}}(r, z, t) = \eta_0(r, z, t) + \eta_2 I(r, z, t) - \frac{\omega_p^2(r, z, t)}{2\omega_0^2}. \quad (8)$$

Here, the first term $\eta_0 = 1 + \delta_1 - i\beta_1$ includes the refraction effect δ_1 and the absorption effect β_1 of neutral atoms, the second term is the Kerr effect, which depends on the intensity of the laser $I(r, z, t)$, and the third term takes into account the contribution of free electrons, the plasma frequency $\omega_p(r, z, t) = [e^2 n_e(r, z, t) / (\epsilon_0 m_e)]^{1/2}$, with m_e and e representing the mass and charge of electron, respectively, and $n_e(r, z, t)$ is the density of free electrons.

The equation for the evolution in the plasma of high-order harmonic field $E_h(r, z, t)$ emitted from atoms located at any position is given by [54]

$$\nabla^2 E_h(r, z, t) - \frac{1}{c^2} \frac{\partial^2 E_h(r, z, t)}{\partial t^2} = \mu_0 \frac{\partial^2 P(r, z, t)}{\partial t^2}, \quad (9)$$

where $P(r, z, t)$ is the polarization depending on the applied fundamental field $E_l(r, z, t)$, which is separated into linear and nonlinear components, and the linear susceptibility $\chi^{(1)}(\omega)$ includes both linear dispersion and absorption effects of the harmonics [56]. The nonlinear polarization term $P_{nl}(r, z, t)$ can be expressed as

$$P_{nl}(r, z, t) = [n_0 - n_e(r, z, t)]D(r, z, t), \quad (10)$$

where n_0 is the density of the initial neutral atom, and $D(r, z, t)$ is the single-atom-induced dipole moment, which can be obtained by Eq. (3). Equations (7) and (9) are solved by the Crank-Nicolson method [53]. Once the harmonic field at the exit face (near field) of the medium is available, the harmonics propagating in free space in the far field can be obtained from near-field harmonics by a Hankel transformation [57,58]

$$\begin{aligned} E_h^f(r_f, z_f, \omega) = -ik \int \frac{E_h(r, z', \omega)}{z_f - z'} J_0\left(\frac{kr r_f}{z_f - z'}\right) \\ \times \exp\left[\frac{ik(r^2 + r_f^2)}{2(z_f - z')}\right] r dr, \end{aligned} \quad (11)$$

where J_0 is the zero-order Bessel function, z_f and z are the far-field and near-field positions from the laser focus, r_f is the transverse coordinate in the far field, and the wave vector k is given by $k = \omega/c$.

D. Macroscopic attosecond pulse generation and time-frequency analysis of propagated high-order harmonics

Macroscopic attosecond pulses in the far field can be obtained by superimposing harmonics in a specific space and energy range, thus the intensity of a far-field attosecond pulse is

$$I_{\text{far}}(t) = \int_0^{r_0} 2\pi r_f dr_f \left| \int_{\omega_1}^{\omega_2} E_h^f(r_f, \omega) e^{i\omega t} d\omega \right|^2. \quad (12)$$

Here, r_0 is the radius of the circular filter, which is perpendicular to the direction of harmonic propagation.

To analyze the time-emission characteristics of harmonics, we perform the time-frequency analysis in terms of the wavelet transform of the harmonic field [59,60]:

$$A(t, \omega) = \int E_h(t') w_{t,\omega}(t') dt' \quad (13)$$

with the wavelet kernel $w_{t,\omega}(t') = \sqrt{\omega} W[\omega(t' - t)]$. The Morlet wavelet is chosen as [59]

$$W(x) = (1/\sqrt{\tau}) e^{ix} e^{-x^2/2\tau^2}. \quad (14)$$

Here τ is a constant. We choose $\tau = 15$ to perform the wavelet transform in this paper.

III. RESULTS AND DISCUSSION

A. Comparison of HHG and attosecond pulses generated from neon atoms driven by optimized multicolor laser fields

In order to explore the influence of the driving field synthesized with different number of components on the emission of high-order harmonics and the corresponding attosecond pulses from neon atoms, we first optimize the waveform for the two-color near-infrared fields combination (800 nm and 1300 nm) with total laser intensity of 7.0×10^{14} W/cm² by GA, as depicted with the solid red line shown in Fig. 1(a). The corresponding laser parameters are given in the second column of Table I. It can be seen from the Fig. 1(a) that a subperiodic pulse is obtained by coherently synthesizing two 16 fs infrared lasers. The HHG spectrum generated from neon atoms in the optimized two-color laser field is given by

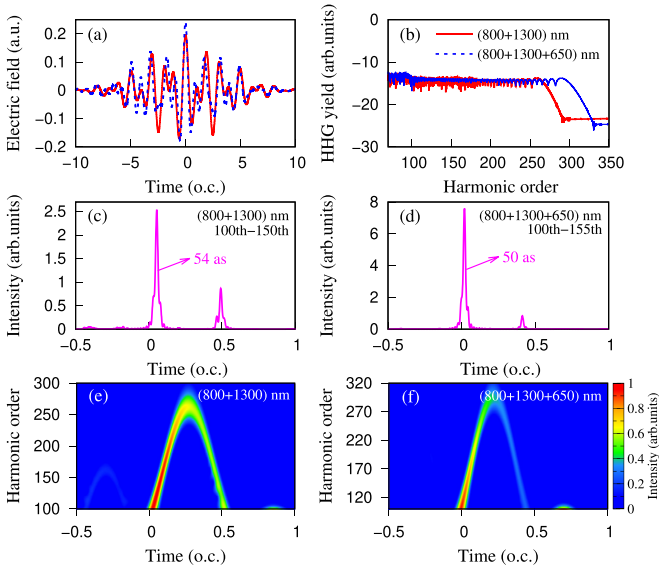


FIG. 1. (a) Waveforms of optimized two- (red solid line) and three-color (blue dashed line) laser fields. (b) HHG spectra obtained from optimized two- (red solid line) and three-color (blue solid line) laser fields, respectively. (c) and (d) The temporal profile of attosecond pulses synthesized from 100th–150th and 100th–155th harmonics for two- and three-color fields, respectively. (e) and (f) Time-frequency analysis of the normalized harmonic spectra generated by optimized two- and three-color field. o.c. is the optical cycle of 800 nm laser pulse.

the solid red line in Fig. 1(b). It can be seen that the supercontinuum spectrum covering from 100th–260th harmonics is obtained. Figure 1(c) shows the temporal profile of the attosecond pulse by superposing the 100th–150th harmonics. As can be seen, two attosecond pulses with different intensities are obtained, where the width of the stronger pulse is about 54 as. The time-frequency distribution is presented to further understand the emission characteristics of these

TABLE I. Optimized laser parameters for two-, three-, and four-color fields with total peak intensity of $7.0I_0$. We mention that the optimized electric field amplitudes can be easily converted to the corresponding laser intensities in unit of $I_0 = 10^{14}$ W/cm². The FWHM duration of each laser is 16 fs. The optimized values are in italics. The numbers in regular font are fixed parameters in the optimization.

Parameter	Two-color	Three-color	Four-color
λ_1 (nm)	800.0	800.0	800.0
λ_2 (nm)	1300.0	1300.0	1300.0
λ_3 (nm)		650.0	400.0
λ_4 (nm)			650.0
$I_1(I_0)$	<i>3.482</i>	<i>1.848</i>	<i>0.434</i>
$I_2(I_0)$	<i>3.518</i>	<i>2.715</i>	<i>0.922</i>
$I_3(I_0)$		<i>2.437</i>	<i>3.851</i>
$I_4(I_0)$			<i>1.793</i>
t_{d1} (fs)	0.0	0.0	0.0
t_{d2} (fs)	<i>0.224</i>	<i>0.105</i>	<i>2.892</i>
t_{d3} (fs)		<i>-2.174</i>	<i>0.583</i>
t_{d4} (fs)			<i>-0.224</i>

attosecond pulses, which is shown in Fig. 1(e). Clearly, the stronger attosecond pulse is emitted from short trajectories with a positive attochirp, while the weaker one is from long trajectories with a negative attochirp. It has been shown that the pulse contributed from long trajectories will be significantly suppressed and only the isolated attosecond pulse emitted from short trajectories will be retained when the harmonics undergo macroscopic evolution by putting the gas target after the laser focus [61,62]. In order to shorten the width of the attosecond pulses generated by the optimized two-color near-infrared laser field, we propose to add a second harmonic field of 1300 nm (i.e., 650 nm) to a two-color near-infrared laser. The optimized waveform of three-color laser field is given by the blue dashed line in Fig. 1(a), and the corresponding laser parameters are listed in the third column of Table I. Compared with the optimized two-color near-infrared laser field, the electric field waveform of the optimized three-color field does not change significantly, especially in the main emission region of attosecond pulses (i.e., near $t = 0$). The HHG spectrum from Ne atoms driven by an optimized three-color laser field is shown in the blue line in Fig. 1(b). It can be seen that the harmonic cutoff energy is extended from the 260th to the 290th harmonic and the supercontinuum spectrum in the harmonic plateau region is smoother when the second harmonic field of the 1300 nm pulse is added, which will be more favorable for generating IAPs. The shortest attosecond pulse obtained by superimposing 100–155th harmonics is shown in Fig. 1(d). We can see that the IAP with the duration of 50 as is created. Figure 1(f) present the corresponding time-frequency analysis of the HHG spectrum. Compared with Fig. 1(e), the harmonic contributions from long electron trajectories are dramatically suppressed. This is beneficial for the generation of the IAPs. However, the harmonic chirp is not greatly reduced.

Can we reduce the inherent attochirp in harmonic emission for shortening the attosecond pulse? We further add the second harmonic field of 800 nm laser to form the so-called four-color synthetic field. The parameters of the optimized four-color laser field are given in the fourth column of Table I, and the synthesized subperiodic waveform is shown in Fig. 2(a). The harmonic spectrum generated by the optimized four-color field is given in the red line of Fig. 2(b). It can be seen that the harmonic spectrum has a good supercontinuity in the range of 80th–170th harmonics, and a single pulse of quasi-chirp-free 37 as is obtained by superimposing the 100th–165th harmonics in the plateau region [see Fig. 2(c)]. Note that the corresponding Fourier-transform-limited pulse width is about 36 as. Compared with the optimized three-color field, it can be found that the width of the attosecond pulse obtained by the optimized four-color synthesis field is significantly shortened. To understand the reason for obtaining the quasi-chirp-free IAP, we perform the time-frequency analysis for the harmonic spectrum driven by the four-color synthetic field as shown in Fig. 2(e). It can be found that the harmonic spectrum of neon atomic emission driven by the optimized four-color field has very distinctive features: First, the contribution of long electron trajectories to the harmonics is completely suppressed. Second, the chirp-free emission is almost achieved in the 100th–165th harmonic range, which means the harmonics with different energies are

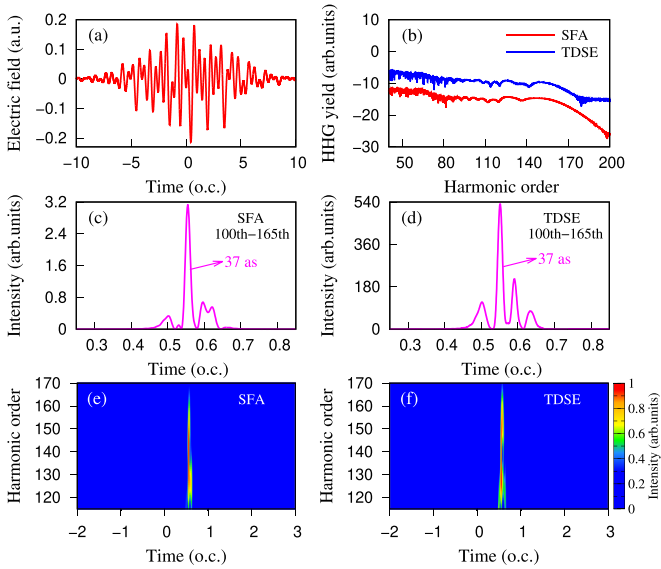


FIG. 2. (a) Laser waveform of optimized four-color laser field. (b) Harmonic spectra obtained using the SFA (red solid line) and TDSE (blue solid line) methods. (c) and (d) The IAPs with the SFA and TDSE methods obtained by synthesizing high harmonics in the same energy region of 100th–165th. (e) Time-frequency image for the harmonic spectrum calculated with the SFA method. (f) Same as (e), but with the TDSE model.

emitted almost at the same time. To verify the results calculated by the SFA model, we calculated HHG spectra and IAPs with the time-dependent Schrödinger equation (TDSE) [63] in Figs. 2(b) and 2(d). As can be seen in Fig. 2(b), the HHG spectrum calculated with the SFA model (red solid line) agrees very well with the TDSE results (blue solid line). The IAP obtained by superimposing the same energy range harmonics from the TDSE is shown in Fig. 2(d). The IAP with the same pulse duration is obtained and the temporal profile is very similar with that obtained by the SFA. To get a deep insight, we further perform the time-frequency analysis for the HHG spectra from the TDSE, as shown in Fig. 2(f). Comparing with Fig. 2(e), it can be seen that the time-frequency characteristics calculated with the SFA model agree well with that based on the TDSE simulation.

To understand the generation of the quasi-chirp-free high-order harmonics and IAPs, we conduct classical analysis as in Refs. [41,42] by solving the classical Newton's equation $\ddot{x}(t) = -E(t)$. The relationship between the ionization time and the recombination time of electrons and the electron energy in the optimized four-color field are shown in Fig. 3(a). It can be seen that there are multiple electron paths with different ionization instants (marked as $i_1 - i_7$) for a given energy when the kinetic energy of the electron is greater than 155 eV (corresponding to the 100th harmonic), and the electron recombination times for these different paths are almost the same. Next, we take four trajectories (i_1, i_3, i_5, i_7) for example to exhibit intuitively how these quasi-chirp-free harmonics are generated. These trajectories are originated from the electrons with different ionized instants returning to the parent ion at the same time near 0.55 o.c., as shown in Fig. 3(b). Furthermore, we also calculate the kinetic energy of the ionized electron as

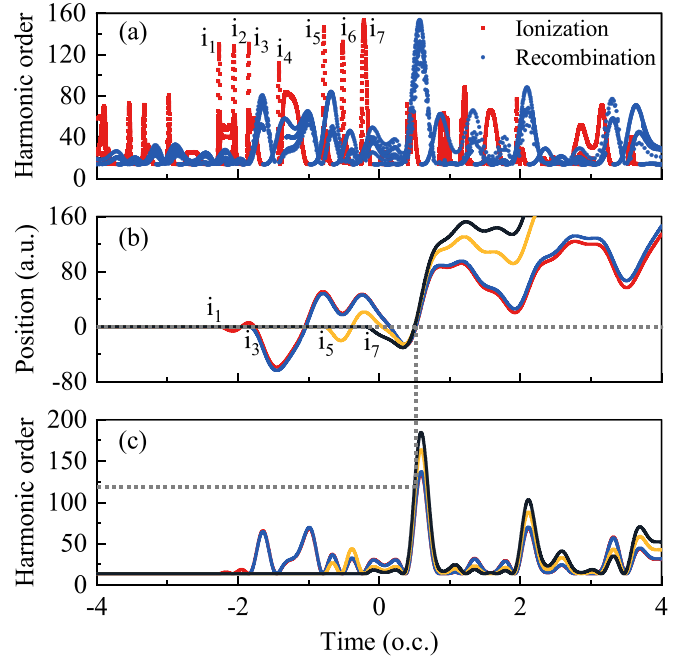


FIG. 3. (a) Classical analysis of electron dynamics in optimized four-color field, $i_1 - i_7$ are the seven ionization events with energies greater than the 80th harmonic. (b) The four classical electron trajectories for the 120th harmonic. (c) Variation of the kinetic energy of the electrons of the four trajectories with the time.

a function of the time shown in Fig. 3(c). It can be observed that the kinetic energy of the returning electron at the instant 0.55 o.c. are almost the same for the above four trajectories, which all contribute to the same order harmonic (i.e., 120th harmonic). These conclusions are consistent with those reported in Refs. [41,42]. Although there is a certain chirp for high-order harmonics larger than 100th, the chirp rate is very small, which is in good agreement with quantum calculations.

B. Effect of gas pressure on macroscopic high-order harmonics and IAPs

In Sec. III A, we comparatively study the influence of driving fields synthesized with different wavelength components on the emission of high-order harmonics and corresponding attosecond pulses from the neon atom at the single-atom level. More importantly, the quasi-chirp-free high-order harmonics driven by the optimized four-color field can be obtained. In experiments, the laser field has a spatial distribution, thousands of atoms in the gas jet feel different laser intensities, and thus the high-order harmonics emitted in space is affected by the macroscopic propagation effect. In order to see whether the quasi-chirp-free high-order harmonics and IAPs can still be generated after macroscopic propagation or not, we solve the 3D Maxwell's wave equations of the optimized four-color laser and high-order harmonic field, respectively. In the present simulations, we use a gas jet with 1 mm width located 2 mm after the laser focal spot and the far-field harmonic signal collector is placed 500 mm behind the focal spot.

It is known that the waveform of a fundamental driving laser is affected by dispersion, Kerr nonlinear effects, and plasma defocusing during propagation. Therefore, one can

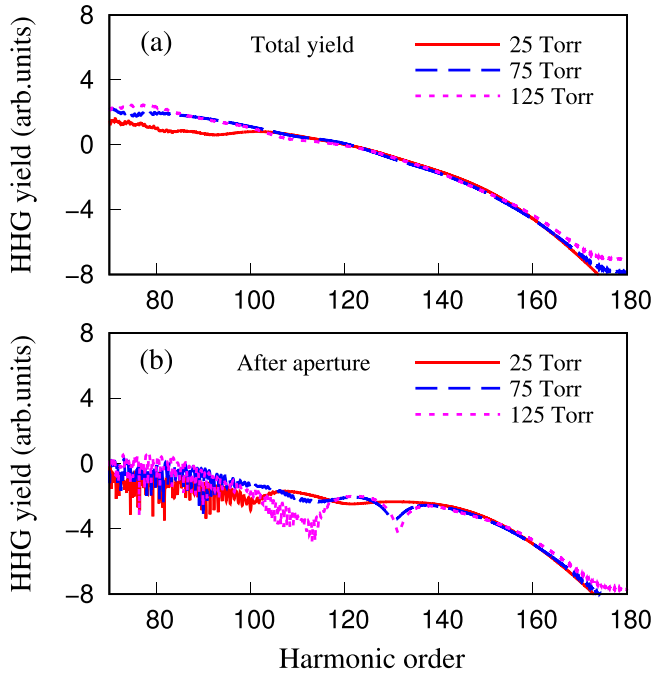


FIG. 4. (a) Total harmonic yields generated by optimized four-color field at different gas pressures. (b) Harmonic yield integrated within 0.15 mm using an aperture at different gas pressures. The macroscopic conditions are: jet width of 1 mm and beam waist of 75 μm . The center of the gas jet is located 2 mm after the laser focal spot.

expect the gas pressure has a significant influence on the macroscopic HHG. We first investigate the effect of gas pressure under a tighter beam waist of 75 μm on the macroscopic harmonics and IAPs generated from neon atoms by the optimized four-color field. We choose the gas pressures of 25, 75, and 125 Torr, and simulate the macroscopic HHG spectra,

as shown in Fig. 4. As can be seen in Fig. 4(a), the total harmonic spectrum of 80th–170th keep the good supercontinuum structures under different gas pressures. Figure 4(b) shows the harmonic spectra collected by a circular filter with a 0.15 mm aperture in the far field for different gas pressures. It is good that the harmonic spectrum in the far field still has a very good supercontinuum in the range of 95th–170th at different gas pressures. Furthermore, it can be found that a significant peak-valley structure appears in the plateau region as gas pressure increases.

To clarify the peak-valley structures in the harmonic plateau region under the higher gas pressures and how it affects the IAPs, the radial distribution of harmonic emission, IAPs, and the time-frequency analysis of on-axis harmonics in the far field for different gas pressures are given in Fig. 5. As can be seen in Figs. 5(a)–5(c), the harmonics are mainly distributed near the propagation axis for three gas pressures (radial distance less than ~ 2 mm, corresponding to the harmonic divergence angle less than 4 mrad). These coherent supercontinuum harmonics with low divergence angle is more conducive to the collection of harmonics and the synthesis of short IAPs. Comparing Figs. 5(a)–5(c), it can be found that the divergence of the harmonic radial distribution slightly increases and the radiation of harmonics around 110th and 130th on the axis is attenuated as gas pressure increases. The increase of harmonic divergence is due to the poor phase matching of harmonic radiation under high pressure. The peak-valley structures in the plateau can be attributed to the destructive interference of different quantum orbitals initiating at different ionization instants, which can be confirmed by comparing Figs. 5(g)–5(i). To confirm whether the quasi-chirp-free IAPs can still be generated in the macroscopic level or not, we superimpose the 95th–165th harmonics to obtain the IAPs with durations of 56 as, 50 as, and 37 as at 25 Torr, 75 Torr, and 125 Torr, respectively [see Figs. 5(d)–5(f)]. It can be seen that the duration of

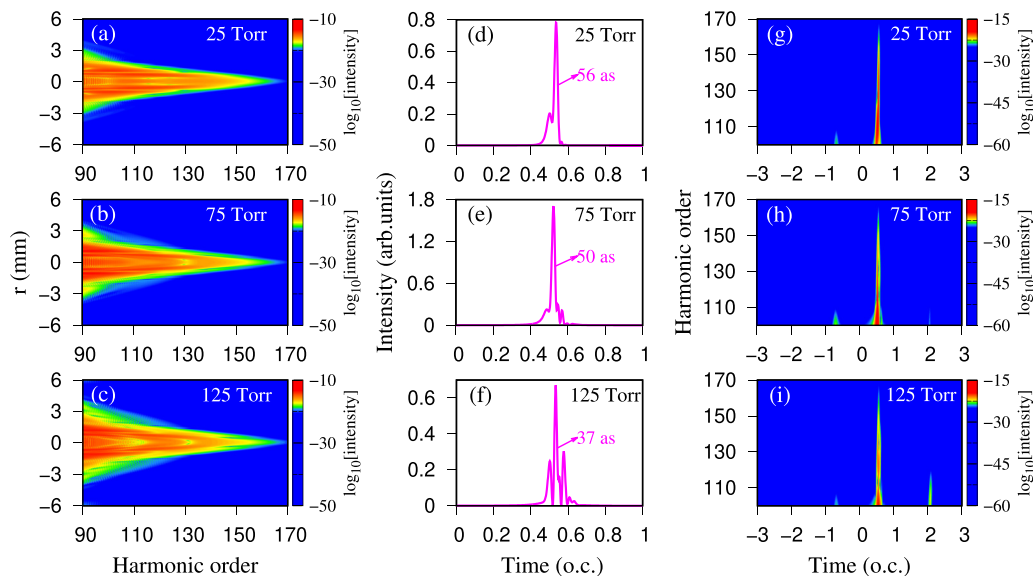


FIG. 5. The spatial distribution of far-field harmonic emission for optimizing the four-color field at different gas pressures: (a) 25 Torr, (b) 75 Torr, and (c) 125 Torr. IAPs synthesized from the 95th–165th harmonics in Fig. 4(b): (d) 25 Torr, (e) 75 Torr, and (f) 125 Torr. Time-frequency analysis for on-axis high-order harmonics in the far field: (g) 25 Torr, (h) 75 Torr, and (i) 125 Torr.

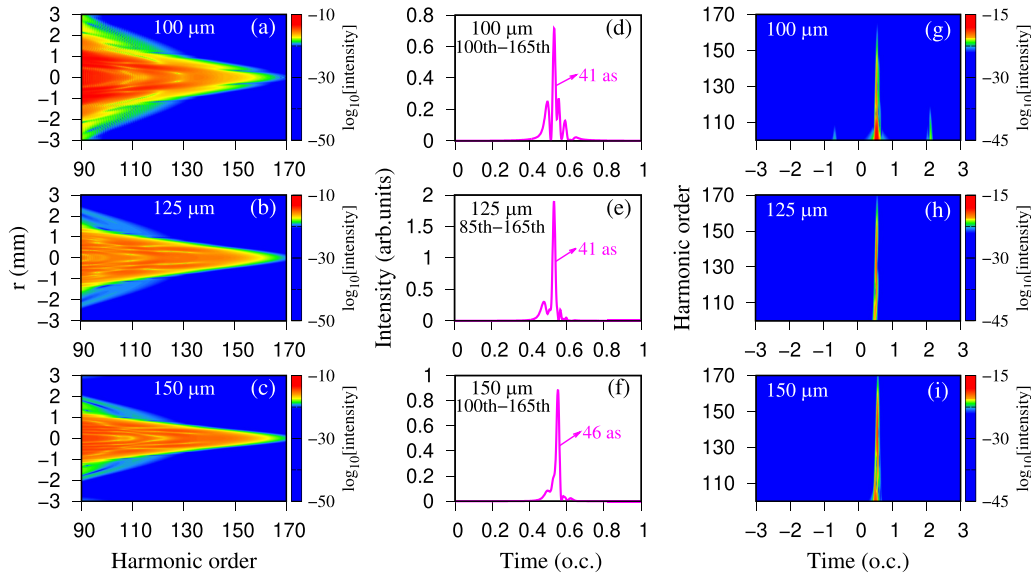


FIG. 6. The spatial distribution of far-field harmonic emission for optimizing the four-color field at the width of three laser beam waist: (a) 100 μm , (b) 125 μm , and (c) 150 μm . Gas pressure and jet position are 100 Torr, 4 mm behind the focal spot, 5 Torr, 2 mm behind the focal spot, and 5 Torr, at the focal spot in (a), (b), and (c), respectively. The IAPs synthesized from 100th–165th, 85th–165th, and 100th–165th harmonics integrated within 0.15 mm using an aperture for three width: (d) 100 μm , (e) 125 μm , and (f) 150 μm . Time-frequency analysis of on-axis high-order harmonics in the far-field for three different widths: (g) 100 μm , (h) 125 μm , and (i) 150 μm .

IAPs gradually decreases with the increasing of gas pressure. To interpret the reduction of the duration of IAPs with gas pressure, we present the time-frequency analysis of on-axis harmonic in the far field at three different gas pressures in Figs. 5(g)–5(i). One can see that the short orbit radiation has a small positive chirp at 25 Torr [see Fig. 5(g)]. As the gas pressure increases, the chirp rate of the short orbit can be reduced and almost chirp-free emission can be achieved in the 100th–170th harmonic range at the proper gas pressure of 125 Torr [see Fig. 5(i)]. The chirp reduction for high gas pressure is due to the self-phase modulation of the fundamental pulse and the chirp compensation of the attosecond harmonic pulse by the dispersion properties of the harmonic generation medium itself [38,64]. Therefore, we can conclude that the quasi-chirp-free high-order harmonics and IAPs from neon atoms driven by an optimized four-color field can still be maintained after propagation at a proper gas pressure.

Finally, we consider the effect of laser beam waist on the macroscopic HHG and IAPs. We choose three widths of 100 μm , 125 μm , and 150 μm and then search the proper jet position and gas pressure to produce the shortest IAP, respectively. The optimal jet positions and gas pressures are 4 mm behind the focal spot and 100 Torr for 100 μm , 2 mm behind the focal spot and 5 Torr for 125 μm , and at the focal spot and 5 Torr for 150 μm , respectively. The radial distribution of harmonic emissions in the far field for three different widths are shown in Figs. 6(a)–6(c). For these three beam widths, we can see that the 90th–170th harmonics have supercontinuum characteristics. In addition, the harmonic divergence gradually becomes smaller as the laser beam waist increases, which is due to the harmonic divergence angle $\theta \propto \lambda/\omega_0$, where λ is the wavelength of the optimized four-color laser field, ω_0 is the laser beam waist. The IAPs synthesized from 100th–165th, 85th–165th, and 100th–165th harmonics inte-

grated within 0.15 mm aperture for three different widths are shown in Figs. 6(d)–6(f). For both 100 μm and 125 μm beam waists, it can be seen that the duration of the shortest IAP generated at optimal parameters is 41 as. For 150 μm , the duration of the shortest IAP is 46 as. One can see that the chirp rate of harmonics from short orbit slightly increases as beam waist increases. Figures 5 and 6 indicate that ultrashort macroscopic IAPs can be generated by optimizing the four-color field at suitable gas pressure and jet position for tightly and loosely focused laser beams. Moreover, we also notice that the chirp rates of high-order harmonics [see Figs. 6(g)–6(i)] and IAPs [see Figs. 6(d)–6(f)] by loosely focused lasers are larger than that of the tightly focused one [see Figs. 5(f) and 5(i)]. This means that the chirped IAPs are generated for these loosely focused laser cases.

IV. CONCLUSION

In summary, we propose an efficient method for generating the broadband (over 100 eV) quasi-chirp-free high-order harmonics and short IAPs from neon atoms by using the optimized four-color laser field synthesized by two fundamental near-infrared lasers and their second-harmonic fields. In accordance with previous findings from a proof-of-principle study [41] and an investigation with two-color laser pulse [42], our classical simulations and the time-frequency analysis show that the reason for generating the quasi-chirp-free high-order harmonics and IAPs for the optimized four-color field case is that the electron ionized at different instants can simultaneously recombine to the parent ion with the same kinetic energy. Furthermore, we also study the propagation effects on the attochirp of high-order harmonic pulses, and find that the quasi-chirp-free isolated IAP can still be obtained

at a proper gas pressure using tightly focused laser beam, while the chirped IAPs are produced in loosely focused lasers.

Even though the optimized laser in this paper is synthesized with four-color lasers, the two fundamental near-infrared and infrared lasers and their second-harmonic fields can be easily obtained by using nonlinear optical crystals, optical parametric amplifier (OPA), and waveform synthesizing technique. For example, parametric waveform synthesizer given in [27] can generate two spectral channels, i.e., 650–1000 nm range and 1200–2200 nm range, respectively,

pumped by a Ti:Sapphire laser, which covers our two fundamental wavelengths. We hope our method can shed more light on the generation of chirp-free IAPs or even isolated subattosecond pulses in experiments.

ACKNOWLEDGMENTS

This work was supported by the National Natural Science Foundation of China under Grants No. 12164044, No. 11964033, and No. 91850209.

-
- [1] A. Föhlisch, P. Feulner, F. Hennies, A. Fink, D. Menzel, D. Sanchez-Portal, P. M. Echenique, and W. Wurth, *Nature (London)* **436**, 373 (2005).
- [2] H. Niikura, F. Légaré, R. Hasbani, A. D. Bandrauk, M. Y. Ivanov, D. M. Villeneuve, and P. B. Corkum, *Nature (London)* **417**, 917 (2002).
- [3] A. Baltuška, T. Udem, M. Uiberacker, M. Hentschel, E. Goulielmakis, Ch. Gohle, R. Holzwarth, V. S. Yakovlev, A. Scrinzi, T. W. Hänsch, and F. Krausz, *Nature (London)* **421**, 611 (2003).
- [4] M. Drescher, M. Hentschel, R. Kienberger, M. Uiberacker, V. Yakovlev, A. Scrinzi, Th. Westerwalbesloh, U. Kleineberg, U. Heinzmann, and F. Krausz, *Nature (London)* **419**, 803 (2002).
- [5] M. Uiberacker, Th. Uphues, M. Schultze, A. J. Verhoef, V. Yakovlev, M. F. Kling, J. Rauschenberger, N. M. Kabachnik, H. Schroeder, M. Lezius, K. L. Kompa, H.-G. Muller, M. J. J. Vrakking, S. Hendel, U. Kleineberg, U. Heinzmann, M. Drescher, and F. Krausz, *Nature (London)* **446**, 627 (2007).
- [6] M. Wu, S. Chen, S. Camp, K. J. Schafer, and M. B. Gaarde, *J. Phys. B* **49**, 062003 (2016).
- [7] T. Popmintchev, M. C. Chen, D. Popmintchev, P. Arpin, S. Brown, S. Alisauskas, G. Andriukaitis, T. Balciunas, O. D. Mücke, A. Pugzlys, A. Baltuska, B. Shim, S. E. Schrauth, A. Gaeta, C. Hernández-García, L. Plaja, A. Becker, A. Jaron-Becker, M. M. Murnane, and H. C. Kapteyn, *Science* **336**, 1287 (2012).
- [8] P. B. Corkum and F. Krausz, *Nature Phys.* **3**, 381 (2007).
- [9] F. Krausz and M. Ivanov, *Rev. Mod. Phys.* **81**, 163 (2009).
- [10] K. J. Schafer, B. Yang, L. F. DiMauro, and K. C. Kulander, *Phys. Rev. Lett.* **70**, 1599 (1993).
- [11] P. B. Corkum, *Phys. Rev. Lett.* **71**, 1994 (1993).
- [12] E. Goulielmakis, M. Schultze, M. Hofstetter, V. S. Yakovlev, J. Gagnon, M. Uiberacker, A. L. Aquita, E. M. Gullikson, D. T. Attwood, and R. Kienberger, *Science* **320**, 1614 (2008).
- [13] F. Ferrari, F. Calegari, M. Lucchini, C. Vozzi, S. Stagira, G. Sansone, and M. Nisoli, *Nature Photon.* **4**, 875 (2010).
- [14] J. Li, X. M. Ren, Y. C. Yin, K. Zhao, A. Chew, E. Cunningham, Y. Wang, S. Y. Hu, Y. Wu, M. Chini, and Z. H. Chang, *Nature Commun.* **8**, 186 (2017).
- [15] S. Gilbertson, S. D. Khan, Y. Wu, M. Chini, and Z. Chang, *Phys. Rev. Lett.* **105**, 093902 (2010).
- [16] X. Wang, L. Wang, F. Xiao, D. Zhang, Z. Lü, J. Yuan, Z. Zhao, *Chin. Phys. Lett.* **37**, 023201 (2020).
- [17] H. Vincenti and F. Quéré, *Phys. Rev. Lett.* **108**, 113904 (2012).
- [18] K. T. Kim, C. Zhang, T. Ruchon, J. F. Hergott, T. Augustine, and D. M. Villeneuve, *Nature Photon.* **7**, 651 (2013).
- [19] T. Gaumnitz, A. Jain, Y. Pertot, M. Huppert, I. Jordan, F. Ardana-Lamas, and H. J. Worner, *Opt. Express* **25**, 27506 (2017).
- [20] J. Tate, T. Augustine, H. G. Muller, P. Salières, P. Agostini, and L. F. DiMauro, *Phys. Rev. Lett.* **98**, 013901 (2007).
- [21] A. D. Shiner, C. Trallero-Herrero, N. Kajumba, H. C. Bandulet, D. Comtois, F. Légaré, M. Giguère, J. C. Kieffer, P. B. Corkum, and D. M. Villeneuve, *Phys. Rev. Lett.* **103**, 073902 (2009).
- [22] G. Cirmi, E. M. Roland, A. S. Miguel, S. Fabian, C. Hüseyin, K. Maximilian, R. G. Maria, and K. X. Franz, *Laser Photon. Rev.* **17**, 2200588 (2023).
- [23] J. R. Pierce, J. P. Palaastro, F. Li, B. Malaca, D. Ramsey, J. Vieira, K. Weichman, and W. B. Mori, *Phys. Rev. Res.* **5**, 013085 (2023).
- [24] S. W. Huang, G. Cirmi, J. Moses, K. H. Hong, S. Bhardwaj, J. R. Birge, L. J. Chen, E. Li, B. J. Eggleton, G. Cerullo, and F. X. Kärtner, *Nature Photon.* **5**, 475 (2011).
- [25] B. Xue, Y. Tamaru, Y. Fu, H. Yuan, P. F. Lan, O. D. Mücke, A. Suda, K. Midorikawa, and E. J. Takahashi, *Sci. Adv.* **6**, eaay2802 (2020).
- [26] P. Huang, S. B. Fang, Y. T. Gao, K. Zhao, X. Hou, and Z. Y. Wei, *Appl. Phys. Lett.* **115**, 031102 (2019).
- [27] G. M. Rossi, R. E. Mainz, Y. Yang, F. Scheiba, M. A. Silva-Toledo, S. H. Chia, P. D. Keathley, S. Fang, O. D. Mücke, C. Manzoni, G. Cerullo, G. Cirmi, and F. X. Kärtner, *Nature Photon.* **14**, 629 (2020).
- [28] R. Bartels, S. Backus, E. Zeek, L. Misoguti, G. Vdovin, I. P. Christov, M. M. Murnane, and H. C. Kapteyn, *Nature (London)* **406**, 164 (2000).
- [29] A. M. Weiner, *Rev. Sci. Instrum.* **71**, 1929 (2000).
- [30] T. Kroh, C. Jin, P. Krogen, P. D. Keathley, A. L. Calendron, J. P. Siqueira, H. K. Liang, E. L. Filho, C. D. Lin, F. X. Kärtner, and K. H. Hong, *Opt. Express* **26**, 16955 (2018).
- [31] C. Jin, G. L. Wang, H. Wei, A.-T. Le, and C. D. Lin, *Nat. Commun.* **5**, 4003 (2014).
- [32] Z. Zeng, Y. Cheng, X. Song, R. Li, and Z. Xu, *Phys. Rev. Lett.* **98**, 203901 (2007).
- [33] P. Lan, P. Lu, W. Cao, Y. Li, and X. Wang, *Phys. Rev. A* **76**, 011402(R) (2007).
- [34] G. Sansone, L. Poletto, and M. Nisoli, *Nature Photon.* **5**, 655 (2011).
- [35] K. Yang, J.-X. Du, G.-L. Wang, Z.-H. Jiao, S.-F. Zhao, and X.-X. Zhou, *J. Opt. Soc. Am. B* **39**, A75 (2022).
- [36] Y. Mairesse, A. D. Bohan, L. J. Frasinski, H. Merdji, L. C. Dinu, P. Monchicourt, P. Breger, M. Kovačev, R. Taïeb, B. Carré,

- H. G. Muller, P. Agostini, and P. Salières, *Science* **302**, 1540 (2003).
- [37] R. López-Martens, K. Varjú, P. Johnsson, J. Mauritsson, Y. Mairesse, P. Salières, M. B. Gaarde, K. J. Schafer, A. Persson, S. Svanberg, C. G. Wahlström, and A. L’Huillier, *Phys. Rev. Lett.* **94**, 033001 (2005).
- [38] K. T. Kim, K. S. Kang, M. N. Park, T. Imran, G. Umesh, and C. H. Nam, *Phys. Rev. Lett.* **99**, 223904 (2007).
- [39] A. S. Morlens, P. Balcou, P. Zeitoun, C. Valentin, V. Laude, and S. Kazamias, *Opt. Lett.* **30**, 1554 (2005).
- [40] Y. H. Zheng, Z. A. Zeng, P. Zou, L. Zhang, X. F. Li, P. Liu, R. X. Li, and Z. Z. Xu, *Phys. Rev. Lett.* **103**, 043904 (2009).
- [41] M. C. Kohler, C. H. Keitel, and K. Z. Hatsagortsyan, *Opt. Express* **19**, 4411 (2011).
- [42] R. X. Yu, Y. Qiao, P. Li, J. Wang, J. G. Chen, W. Feng, F. M. Guo, and Y. J. Yang, *Chin. Phys. B* **32**, 063302 (2023).
- [43] L. E. Chipperfield, J. S. Robinson, J. W. G. Tisch, and J. P. Marangos, *Phys. Rev. Lett.* **102**, 063003 (2009).
- [44] E. Balogh, B. Bódi, V. Tosa, E. Goulielmakis, K. Varjú, and P. Dombi, *Phys. Rev. A* **90**, 023855 (2014).
- [45] C. Jin and C. D. Lin, *Chin. Phys. B* **25**, 094213 (2016).
- [46] M. Lewenstein, P. Balcou, M. Y. Ivanov, A. L’Huillier, and P. B. Corkum, *Phys. Rev. A* **49**, 2117 (1994).
- [47] M. Lewenstein, P. Salières, and A. L’Huillier, *Phys. Rev. A* **52**, 4747 (1995).
- [48] M. V. Ammosov, N. B. Delone, and V. P. Krainov, *Sov. Phys. JETP* **64**, 1191 (1986).
- [49] X. M. Tong and C. D. Lin, *J. Phys. B* **38**, 2593 (2005).
- [50] M. B. Gaarde, J. L. Tate, and K. J. Schafer, *J. Phys. B* **41**, 132001 (2008).
- [51] M. Geissler, G. Tempea, A. Scrinzi, M. Schnürer, F. Krausz, and T. Brabec, *Phys. Rev. Lett.* **83**, 2930 (1999).
- [52] E. Takahashi, V. Tosa, Y. Nabekawa, and K. Midorikawa, *Phys. Rev. A* **68**, 023808 (2003).
- [53] E. Priori, G. Cerullo, M. Nisoli, S. Stagira, S. De Silvestri, P. Villorosi, L. Poletto, P. Ceccherini, C. Altucci, R. Bruzzese, and C. de Lisio, *Phys. Rev. A* **61**, 063801 (2000).
- [54] C. Jin, A.-T. Le, and C. D. Lin, *Phys. Rev. A* **83**, 023411 (2011).
- [55] S. C. Rae and K. Burnett, *Phys. Rev. A* **46**, 1084 (1992).
- [56] B. L. Henke, E. M. Gullikson, and J. C. Davis, *At. Data Nucl. Data Tables* **54**, 181 (1993).
- [57] V. Tosa, K. T. Kim, and C. H. Nam, *Phys. Rev. A* **79**, 043828 (2009).
- [58] L. E. Chipperfield, J. S. Robinson, P. L. Knight, J. P. Marangos, and J. W. G. Tisch, *Laser Photon. Rev.* **4**, 697 (2010).
- [59] X. M. Tong and S.-I. Chu, *Phys. Rev. A* **61**, 021802(R) (2000).
- [60] M. B. Gaarde, *Opt. Express* **8**, 529 (2001).
- [61] P. Antoine, A. L’Huillier, and M. Lewenstein, *Phys. Rev. Lett.* **77**, 1234 (1996).
- [62] P. Salières, B. Carré, L. Le Déroff, F. Grasbon, G. G. Paulus, H. Walther, R. Kopold, W. Becker, D. B. Milošević, A. Sanpera, and M. Lewenstein, *Science* **292**, 902 (2001).
- [63] X. M. Tong and S. I. Chu, *Chem. Phys.* **217**, 119 (1997).
- [64] K. Kovács and V. Tosa, *Opt. Express* **27**, 21872 (2019).